RSC Advances

ROYAL SOCIETY OF CHEMISTRY

www.rsc.org/advances

Iron-copper bimetallic nanoparticles supported on hollow mesoporous silica spheres: An effective heterogeneous Fenton catalyst for orange II degradation

Jing Wang, Chao Liu, Lu Tong, Jiansheng Li*, Rui Luo, Junwen Qi, Yang Li, Lianjun Wang*

[*] J. Wang, C. Liu, L. Tong, Prof. J.S. Li, R. Luo, J.W. Qi, Y. Li, L.J. Wang

Jiangsu Key Laboratory of Chemical Pollution Control and Resources Reuse

School of Environmental and Biological Engineering

Nanjing University of Science and Technology

Nanjing 210094, P.R .China

E-mail: lijsh@mail.njust.edu.cn; wanglj@mail.njust.edu.cn

Abstract Iron-copper bimetallic nanoparticles supported on hollow mesoporous silica spheres as a composite catalyst (FeCu/HMS) was synthesized via a post-impregnation and sodium borohydride reduction strategy. The catalyst was characterized by X-ray diffraction, X-ray photoelectron spectroscopy, nitrogen physisorption, scanning electron microscopy, transmission electron microscopy, fourier transform infrared spectroscopy and zeta potential. The results showed that the FeCu/HMS catalyst possessed hollow mesoporous structure with interior cavity transfixed by mesoporous silica shell. The iron-copper nanoparticles highly dispersed in the matrix of hollow mesoporous silica spheres. For comparison, three other catalysts, including solely iron nanoparticles supported on hollow mesoporous silica spheres (Fe/HMS), solely copper nanoparticles supported on hollow mesoporous silica spheres (Cu/HMS) and iron-copper nanoparticles supported on solid-core structured mesoporous silica spheres (FeCu/MS), were prepared by the similar procedure. To demonstrate the heterogeneous Fenton catalytic performance of the as-synthesized FeCu/HMS, orange II was chosen as a model contaminant. The results showed that 90.2 % of 50 mg/L orange II was removed during 15 min at the reaction conditions of 1g/L catalyst and 13.7mM H_2O_2 in neutral pH and room temperature, and raised to 94.3 % at 2 h. Kinetic analysis showed that the degradation of orange II follows the pseudo-first order and the apparent rate constant of FeCu/HMS was much higher than those of as comparison catalysts. Additionally, it was found that the addition of copper could make the catalyst less pH dependent and keep the high activity (93.8 % orange II removal efficiency) even at alkaline circumstance (pH=9). The remarkable catalytic performance of FeCu/HMS may be ascribed to the synergetic effect of iron and copper and “cavity effect” of the hollow structure. The stability and recoverability of the catalyst were assessed. The results indicated that the catalyst retained high catalytic activity (78.9 % orange II removal efficiency) after 5 consecutive runs. The unique nanostructure and efficient catalytic activity make the catalyst to be a novel and prospective candidate in heterogeneous Fenton chemistry.

Keywords: Hollow mesoporous silica spheres, Heterogeneous Fenton, Iron-copper bimetallic, Cavity effect

1. Introduction

Fenton technology is one of the powerful and promising advanced oxidation processes (AOPs) for the treatment of wastewater containing recalcitrant toxic organic substances such as pharmaceuticals, pesticides, personal care products and organic synthetic dyes.[1] The classical homogeneous Fenton reagent, exploiting the reaction between Fe^{2+}/Fe^{3+} and hydrogen peroxide (H_2O_2), to generate highly reactive species and destroy the organic matters efficiently.[2] However, the major disadvantages of homogeneous Fenton reaction are the generation of a multitude of iron-containing sludge presented in the effluents and the strong acid condition (pH < 3) demanded, which largely limited application of homogeneous Fenton technology.[3-6] To overcome these drawbacks of homogeneous Fenton reaction, heterogeneous Fenton technology has been developed and extensively studied as a promising alternative for AOPs. Nano zero-valent iron(nZVI) and iron oxide minerals are used as heterogeneous Fenton catalyst to activate H_2O_2 for the generation of highly reactive hydroxyl radicals (•OH) and to treat various organic pollutants.[7-11] However, these heterogeneous Fenton catalysts manifest relatively inert activity if operated at high pH values or without external power supplies such as microwave,[12] ultrasound[13] and UV irradiation.[14,15] However, these external supplies require extra cost and energy input, which will increasing the cost for wastewater treatment.

Targeting for enhancing the heterogeneous Fenton catalytic activity, another metal species, copper, which possesses less pH dependent property, has attracted great attention. The combination of copper with iron to fabricate iron-copper bimetallic nanoparticles, which exhibited an improved catalytic activity due to the synergistic effects of two-metal redox couples, has become a hotspot in the field of Fenton chemistry. Nevertheless, for nanoparticles, it inevitable tend to aggregate into larger particles, leading to deterioration of catalytic performance.[16] To tackle the existing problems,

supporting nanoparticles on suitable matrix has been an efficient strategy. Great efforts have been devoted to incorporate iron-copper bimetallic nanoparticles on a variety of supports, such as zeolite,[17] clay,[18] PAN fiber,[19] MCM-41,[20] ZSM-5[21] and ordered mesoporous carbon materials.[22] However，the nanoparticles in these supports are basically in a two-dimensionally confined space, which would limit the efficient of reaction between the contact interfaces for reactants.[23]

Hollow mesoporous silica spheres (HMS), which have an interior cavity transfixed by mesoporous silica shell, have stimulated extensive interest due to their unusual structural features, including low density, high surface area, good permeation and outstanding optical/electrical behaviors.[24-27] Particularly, the "open" shell morphology and hollow interior allows the substrates more easy access to the active sites.[28] Additionally, their inner- and outer-shell surfaces facilitate contact with reactant molecules.[29,30] Therefore, there is reason to believe that HMS can be a promising support for the immobilization of iron-copper bimetallic nanoparticles, which may be exploited as an excellent candidate in application of heterogeneous Fenton catalysis.

In this study, the iron-copper bimetallic nanoparticles supported on HMS as a composite catalyst (FeCu/HMS) was prepared through the post-impregnation and sodium borohydride reduction strategy. To present the Fenton catalytic performance of FeCu/HMS, a typical azo dye in textile industry, Orange II, was chosen as the model pollutant in catalysis reaction. The main purpose of this study is to elucidate the role of copper and iron and the effect of hollow structure on the catalytic activity in the heterogeneous Fenton reaction. For comparison, three other catalysts, including solely iron nanoparticles supported on hollow mesoporous silica spheres (Fe/HMS), solely copper nanoparticles supported on hollow mesoporous silica spheres (Cu/HMS) and iron-copper nanoparticles supported on solid-core structured mesoporous silica spheres (FeCu/MS), were prepared by the same reduction way. Additionally, the possible mechanism was proposed on

the basis of the detected •OH radical and the surface reaction revealed by comprehensive characterizations. Finally, the stability and reusability of the catalyst was evaluated.

2. Experimental

2.1. Chemicals

Analytical reagents of anhydrous ethanol, concentrated ammonia aqueous solution ($NH_3 \cdot H_2O$, 25 wt %), tetraethylorthosilicate (TEOS), cetyltrimethylammonium bromide (CTAB), ferrous sulfate ($FeSO_4 \cdot 7H_2O$), copper nitrate ($Cu(NO_3)_2 \cdot 3H_2O$), sodium borohydride ($NaBH_4$), hydrogen peroxide (H_2O_2, 30 wt%), sodiumhydroxide (NaOH), nitric acid (HNO_3, 65 wt%) and Acid Orange II ($C_{16}H_{11}N_2NaO_4S$) were purchased from Sinopharm Chemical Reagent Co., Ltd. Titanyl sulphate was purchased from Aladdin Industrial Corporation. Benzoic acid (BA) and p-hydroxy benzoic acid (PBA) were purchased from ANPEL Scientific Instruments (Shanghai) Co., Ltd. All chemicals were used as received without any further purification. Deionized water (Millipore) with a resistivity of 18 MΩ·cm was used in all experiments.

2.2. Synthesis of hollow mesoporous silica spheres

The hollow mesoporous silica spheres were prepared according to the previous literature.[31] In a typical procedure, CTAB was dissolved in ethanol aqueous solution containing concentrated ammonia aqueous solution (1 mL, 25 wt %). Then, the mixture was heated to 35 °C, and TEOS (1 mL) was rapidly added under vigorous stirring. The molar ratio of the reaction mixture was 1.00 TEOS: 0.0922 CTAB: 2.96 NH_3: 621 H_2O: 115 C_2H_5OH. After stirring at 35 °C for 24 h, the white product was collected by centrifugation at 4000 rpm for 10 min and washed three times with ethanol. To prepare the mesoporous silica hollow spheres, the as-made Stöber silica spheres were incubated in pure water (160 mL) at 70 °C for 12 h and then collected by centrifugation and washed three times with ethanol. The products were filtered and dried at 100 °C. Finally, the CTAB

templates were removed by calcination in a muffle furnace at a rate of 1°C /min to 550 °C, holding for 6 h. The calcined samples were denoted as HMS. In comparison, the solid-core structured mesoporous silica spheres, denoted as MS, were prepared in the same Stöber solution without the water incubating process.

2.3. Synthesis of iron-copper bimetallic composite catalysts

The FeCu/HMS bimetallic composites were prepared by a direct impregnation and chemical reduction method. Briefly, 0.1 g of HMS was added into 5 mL aqueous solution containing 20 mg $FeSO_4$ and 15mg Cu $(NO_3)_2$, then stirring for 1h under N_2 atmosphere. The concentration of $FeSO_4$ and Cu $(NO_3)_2$ solutions were 4g/L and 3 g/L, respectively. The theoretical mass percentage of both Fe and Cu on HMS were 3.7 wt%. The suspension then was dried under vacuum at 50 °C, followed by the addition of 1 mL of fresh $NaBH_4$ aqueous solution with stirring for 3h under N_2 atmosphere. The molar ratio of B/(Fe+Cu) was 6/1 with adequate $NaBH_4$ for the formation of iron and copper nanoparticles. The resulted products were immersed in methanol for 12h. The obtained catalysts were collected by filtration and washed with methanol for three times. The final products were denoted as FeCu/HMS. The FeCu/MS was synthesized by the same impregnation and reduction methods except for using solid-core structured mesoporous silica spheres as matrix. The Fe/HMS and Cu/HMS were fabricated by the same strategy with adding the corresponding precursor in impregnation procedure, respectively. The theoretical mass percentage of Fe or Cu on composite catalysts was 7.4 wt%.

2.4. Characterization

The crystalline phase of the samples was identified by X-ray diffraction (XRD) patterns on a Bruker AXS D8 advance powder diffraction system using Cu Kα (λ = 1.5418 Å), operating at 40 kV and 40 mA. The mesoporous phases of the samples were identified at the range of 0.6–8^o with

the scanning speed of 0.01 °/s. Wide diffraction angle analysis was conducted at the range of 10–95° by the same XRD instrument. The X-ray photoelectron spectra (XPS) spectra were obtained by using a PHI Quantera II ESCA System with Al Kα radiation at 1486.8 V. Nitrogen adsorption-desorption isotherms were collected at 77 K using a Micromeritics 2020 analyzer (USA). Before measurements, the samples were degassed in a vacuum at 250 ℃ for 4h. The Brunauer-Emmett-Teller (BET) method was utilized to calculate the specific surface areas (S_{BET}). By using the BJH model, the pore volumes and pore size distributions were derived from the adsorption branches of isotherms, and the total pore volumes (V_t) were estimated from the adsorbed amount at a relative pressure P/P_0 of 0.99. The surface morphology of various samples were examined by Quanta 250F scanning electron microscope (SEM) at an accelerating voltage of 20 kV. Transmission electron microscopy (TEM) images were collected by using a JEOL JEM-2100 microscope (200 KV). The samples were suspended in ethanol, and then dropped on the holey carbon film supported on a Cu grid. STEM-EDS images were performed by FEI Tecnai F30 field emission electron microscope (equipped with an energy-dispersive spectromet er, EDS) at 300 kV. The surface charges of all the samples were measured by Zeta Potential Analyzer (ZetaPALS, Brookhaven Instruments, USA) based on electrophoretic mobility of the nanoparticles in aqueous media at different pH values, and pH was adjusted by using disodium hydrogen phosphate - citric acid buffer with 0.01 M KCl solution as a background electrolyte. Fourier Transform Infrared (FT-IR) spectra of samples were obtained by using FT-IR- Nicolet IS-10 Thermo Fisher. To determine the metal loading contents in samples, all samples were digested by dilute nitric acid solution, then the mixture were filtered through 0.22 μm membrane filter and the metal ion containing filtrates were analyzed by inductive coupled plasma atomic emission spectroscopy (ICP-AES) (Optima 7000DV, PerkinElmer, USA). The iron ions leaching of samples

were determined by atomic absorption spectrometer (AAS) (PinAAcle 900T, PerkinElmer, USA).

2.5. Catalytic performance

A series of batch experiments were carried out to measure the catalytic activity of the samples by degrading Orange II in aqueous solutions. In a typical experiment, 0.01 g of catalyst was added into 10 mL of Orange II solution in a flask (50 mL). The pH of the reaction medium was adjusted by using an appropriate amount of 0.1 M NaOH or 0.1 M HNO_3 to a given value. The covered flasks were kept at a mild temperature (30 ℃) in a thermostatic air bath oscillator with a constant speed of 200 rpm. Then, a certain concentration of H_2O_2 (30 wt%) was added to the suspension and initiated the degradation reaction. Each flask was taken out from the water bath at different time intervals and the supernatant solution was collected by filtration for UV-vis absorbance analysis using a universal microplate spectrophotometer (PowerWave XS). The used catalyst was collected by magnet and regenerated by washing with methanol for stability tests. The quantitation of hydroxyl radicals were determined with method which was reported in the previous literature.[32] For the determination of H_2O_2 concentrations, photometric measurements were performed (at a wavelength of 404 nm) using a solution of titanyl sulphate and a universal microplate spectrophotometer (PowerWave XS). The degradation products of Orange II were detected by high-performance liquid chromatograph (HPLC)-mass spectrometer (MS) (Agilent 6410, Agilent Technologies Incorporation, USA), using Agilent Eclipse Plus-C18 columns (3.5μm, 2.1×150 mm).

3 Results and discussion

3.1. Morphology and physicochemical properties of catalysts

The low-angle and wide-angle XRD patterns of all samples are shown in Fig. 1. In the low angle range (Fig. 1A), the XRD pattern of pure HMS and MS exhibit an intense reflection at low 2θ,

which are typical of worm-like ordered pore structures similar to the previous works.[33] It is worthy to note that the reflection of HMS possesses lower 2θ compared with MS, which may be contributed to the larger mesopore size formed during incubation process in water.[31] With the incorporation of metal species, the peak intensities of the modified samples decrease, suggesting that a less ordered structure was formed and the ordered mesoporous framework of the materials still remain.[34,35] In the wide angle XRD patterns (Fig. 1B), the broad peak at about 22.8° refers to amorphous silica. In Fe/HMS and Cu/HMS samples, an obvious diffraction peak at 44.6° and 43.2° can be observed, which is in accordance with the (110) diffraction of body-centered cubic α-Fe (JCPDS No. 06-0696) and (111) reflections of copper (JCPDS No. 99-0034), respectively. Differently, for iron-copper containing samples, only weaker and broader diffractions at 43.2° and 44.6° can be found. It may be attributed to low metal loading mass and small metal particles depositing on mesoporous silica spheres, which is similar to the previous reports.[20,35] The iron and copper elements composition can be further verified by XPS results. In three iron-containing samples (Fig. 2A), the photoelectron peaks at 706.3 eV representing the binding energy of zero-valent iron (Fe $2p_{3/2}$).[36] As we know, zero-valent iron can be oxidized easily when exposed in air. Thus, the other photoelectron peaks at round 711.0 and 724.6 eV representing the binding energies of Fe $2p_{3/2}$ and $2p_{1/2}$, respectively, indicating the nanoparticles was enveloped by a layer of iron oxides.[37,38] The high-resolution XPS spectra of Fe 2p (Fig. S1) can be curve-fitted into four-type peaks. Particularly, photoelectron peaks at 709.4 and 722.9 eV corresponded to the binding energy of Fe^{2+} $2p_{3/2}$ and $2p_{1/2}$, respectively. The photoelectron peaks at 711.7 and 725.4 eV represented the binding energy of Fe^{3+} $2p_{3/2}$ and $2p_{1/2}$, respectively. And the ratio of Fe^{2+} / Fe^{3+} for FeCu/HMS, FeCu/MS and Fe/HMS are 0.993, 0.992 and 0.992, respectively. In Fig. 2B, it can be observed that two main bands are centered at 932.3 eV (Cu$2p_{3/2}$), 952.1 eV(Cu $2p_{1/2}$), which are

corresponding to binding energy of zero-valent copper in three copper-containing samples.[39] The XPS results demonstrate that the active components of catalysts are zero-valent iron-copper bimetallic.

SEM and TEM of blank samples can be observed in Fig. 3. The as-synthesized HMS and MS possess a spherical morphology with smooth surface and uniform diameter of about 560 nm by the SEM images (Fig. 3A, D). To further explore the difference of interior construction between HMS and MS, TEM images have been shown in Fig. 3B, C, E, F. A noticeable contrast between the cavity and the shell is observed in Fig. 3B, which verifying the hollow structure of HMS. It can also be observed that the HMS have an average diameter of about 560 nm and a mean shell thickness of 75 nm, which in accord with the results of SEM. The formation of hollow sphere is based on solid-to-hollow spontaneous transformation mechanism.[31] Specially, uniform solid-core mesostructured silica spheres were prepared via a surfactant assembly sol−gel process in a Stöber solution containing CTAB, TEOS, ammonia, and ethanol. Then, during incubation process in water, the solid-core structured silica spheres spontaneously transformed into hollow structured silica spheres. The selective etching the inner silica section occurred due to the relative low degree of condensation. Finally, mesoporous silica hollow spheres were obtained by calcination in air. The SEM images of hollow sphere before and after removal of templates were given in Fig. S2. The results show that the hollow spheres have been obtained before the template removal. High-magnification TEM image shows that the mesochannels of the spheres are continuous throughout the shell with openings at surface and are radially oriented to the sphere surface (Fig. 3C), which means that the mesochannels of the hollow spheres are readily accessible. It favors the supported active components contact with reactant molecules. In contrast, the solid-core structured mesoporous silica spheres merely possess oriented mesochannels to the core without cavity (Fig. 3E,

F).

After incorporation of metal nanoparticles by impregnation−reduction approach, the SEM and TEM images of FeCu/HMS, FeCu/MS, Fe/HMS and Cu/HMS can be observed in Fig. 4. SEM images show that composite catalysts retain the spherical morphology with some metal nanoparticles sticking on the outer shells (Fig. 4A, C, E, G). To further investigate the metal nanoparticles dispersion and interior structure of the as-synthesized materials, TEM images have been shown in Fig. 4B, D, F, H. The results show that impregnation of metal nanoparticles has no significant influence on the the silica sphere and shell. Moreover, the sphere and shell in FeCu/HMS, Fe/HMS and Cu/HMS show the extremely same average diameter (560nm for sphere, 75nm for shell, respectively). The dark spots are observed, corresponding to metallic nanoparticles, which are highly dispersed in the matrixes. The average sizes of metal nanoparticles in FeCu/HMS, FeCu/MS, Fe/HMS and Cu/HMS are approximate 18, 19, 30 and 32nm, respectively (Fig. S3). To further explore the distribution of iron and copper in sample FeCu-HMS, the STEM and Energy-dispersive X-ray spectroscopy (EDS) elemental mapping have been performed (Fig. S4). It can be observed that iron and copper are uniformly distributed on the silica matrix.

Nitrogen adsorption-desorption isotherms of the samples are illustrated in Fig. 5A. All of samples exhibit type IV N_2 adsorption isotherms, revealing characteristics of mesoporous materials with narrow pore size distribution.[31] In addition, compared to the solid-core structured mesoporous silica materials, the isotherms of hollow mesoporous silica materials show a hysteresis loop at higher relative pressure (P/P_0 >0.8). The observed loop reflect the macroporous structure of particles, indicating the presence of interior cavity in hollow mesoporous spheres,[40] which in according with the TEM observation. Moreover, the inflection at P/P_0 =0.2-0.3 in the isotherms become weaker after the metal incorporation, which suggests the decreasing order of mesoporous

structures. This phenomenon is consistent with the XRD results. The BET surface area and pore volume of FeCu/HMS (578 $m^2 g^{-1}$, 0.41 $cm^3 g^{-1}$), Fe/HMS (592 $m^2 g^{-1}$, 0.41 $cm^3 g^{-1}$), Cu/HMS (576 $m^2 g^{-1}$, 0.41 $cm^3 g^{-1}$) and FeCu/MS (695 $m^2 g^{-1}$, 0.35 $cm^3 g^{-1}$) are lower than those of blank HMS (765 $m^2 g^{-1}$, 0.56 $cm^3 g^{-1}$) and MS (1007 $m^2 g^{-1}$, 0.49 $cm^3 g^{-1}$) (Table 1). It should be attributed to increment of sample density after loading metals, suggesting successful incorporation of metal species on blank silica spheres. The pore size distribution derived from the adsorption branch for all samples is shown in Fig. 5B. The BJH average pore size of FeCu/HMS (2.31 nm), Fe/HMS (2.31 nm), Cu/HMS (2.31 nm) and FeCu/MS (1.98 nm) are also lower than those of blank HMS (2.51 nm) and MS (2.13 nm), which should be due to the incorporation of metals in mesopore channels. Composition of active species can be further verified by ICP-AES (Table 2), the metal loading contents of all the samples were approached to the theoretical value, further indicating that the metal active species were supported on blank silica spheres successfully.

Fig. 6 shows the FT-IR spectra of various samples. All samples show the characteristic bands at around 796 and 1060 cm^{-1}, which correspond to the symmetric and anti-symmetric Si-O stretching. The absorption band centering at 1630 cm^{-1} and the broad band between 2900 and 3700 cm^{-1} observed for all samples are assigned to the bending and stretching vibration of –OH, which from the dissociative chemisorption of water molecules.[41-43] It is worthy to note that the –OH absorption band intensity obviously enhanced with incorporation of iron, copper and iron-copper, indicating that more surface hydroxyl groups were formed after addition of metals in blank silica sphere. It may be ascribed to the enhanced acid sites of catalyst, which are the results of the tetrahedral framework iron or copper atoms and extra-framework oxide clusters (acidic oxygen-containing surface groups) on the surface of mesoporous silica sphere shells.[42] On this basic, the catalyst could adsorb more hydroxyls from the water molecules with enhanced surface acidity.

The amount of surface acidic oxygen-containing groups existing in the samples can be estimated by measuring zeta potentials (Fig. 7). The point of zero charge (PZC) of blank HMS and MS are at pH =3.2 and 3.4. With the iron, copper and iron-copper incorporation, the PZC shifted to lower pH values (2.7 for Fe/HMS, 2.6 Cu/HMS, for 2.2 for FeCu/HMS, 2.4 for FeCu/MS) (Table 3). The decreased PZC values of modified samples indicated that surface acidic groups increased with addition of metals, leading to the formation of more surface hydroxyl groups,[44] which is consistent with FT-IR results.

3.2. Catalytic degradation performance on orange II of various catalysts

To evaluate the catalytic activity of various catalysts under the conditions of neutral pH value and room temperature, the preliminary experiments on degradation of 50 mg/L orange II were executed at the conditions of H_2O_2 13.7 mM, catalyst dosage 1g/L, pH at 7.0, at 30 degree Celsius. All of the reactions were carried out in the dark to avoid the impact of light. Fig. 8A shows the evolution of orange II abatement within the reaction time for these experiments. It can be seen from that catalyst blank (without the addition of catalyst and only using H_2O_2 as the oxidant) got 30.6 % of orange II reduction after 2 h reaction. Meanwhile, using Fe/HMS or Cu/HMS as the catalyst got 31.6 % or 85.7 % of orange II reduction after 2 h reaction, which reflected that the relative inert catalytic activity of Fe/HMS compared with Cu/HMS. Significantly, almost 90.2 % of 50 mg/L orange II was removed during 15min by FeCu/HMS and raised this value to 94.3 % at 2h, which clearly evidenced the synergetic effect of iron and copper in Fenton reaction.[45] Moreover, in order to investigate the influence of cavity effect on orange II removal, the catalyst FeCu/MS with solid-core mesoporous structure was used. Comparing with FeCu/HMS, FeCu/MS showed lower performance (84.7%) of orange II reduction. In addition, the amount of iron ions leaching after reaction 2h for FeCu/HMS, FeCu/MS and Fe/HMS were also measured by AAS. Few iron ions

were detected (Fig. S5). The amount of iron ions leaching of FeCu/HMS, FeCu/MS and Fe/HMS were measured to be 0.034, 0.046 and 0.064 mg/L, respectively. It can also be seen that the iron ions leaching of FeCu/HMS was lower than FeCu/MS and Fe/HMS. The above results of orange II reduction indicate that FeCu/HMS shows more efficient catalytic activity and stability which may due to iron-copper active component and distinctive hollow structure of the catalyst.

In the mean time, the data for orange II removal were further analyzed by kinetic equation (Fig. 8B). The kinetics equation may be express as

$$\ln(\frac{C_0}{C})=kt$$

where k is the apparent reaction constant, C_0 and C are the initial concentration and the concentration at time t of orange II, respectively. The pseudo-first order reaction kinetics were observed and applied to all experiments. A three-stage reaction occurred in the orange II degradation process by the catalysts (Fig. S6). The reaction kinetics constant of initial stage (0-5min) k_1, second stage (5-15min) k_2 and third stage (15-120min) k_3 for catalysts are illustrated in Table 4. Normally, the degradation of orange II in heterogeneous reaction involves three steps. The first step is adsorption of orange II on the reactive sites of catalysts, the second step is degradation reaction, and the third step is release of degradation products.46 As shown in Fig. S6, the reaction rates in all catalysts become slower from initial stages to third stages, which is different from the performance of photo catalysis.[47,48] That may be ascribed to the following reasons: in the initial stage, all of the active sites were free. H_2O_2 and dye molecules could rapidly reach the active sites. Then, the dye molecules were degraded by hydroxyl radicals with release of degradation products. In the second stage, the reaction rate was limited by the mass transport rates of intermediates, products and reactants between solution phase and catalyst surfaces. In the third stage, the mass transport limited effects became more serious. The similar results were also obtained by the previous reports for

degradation of orange II.[46,49] Obviously, the reaction kinetics constant of FeCu/HMS is more rapid than FeCu/MS, Cu/HMS and Fe/HMS at every stage, which indicating the superiority of catalytic rate for FeCu/HMS. In addition, the possible degradation products of orange II by FeCu/HMS Fenton heterogeneous system were identified by HPLC-MS analysis (Fig. S7, Table S1). As shown in Fig. S7B, five new peaks appeared compared to orange II diagram (Fig. S7A), corresponding to five degradation products. The five possible products were listed in Table S1.

3.3. Effect of the initial pH of the orange II aqueous solution

As we know, the initial pH of the reaction system is seriously affects the catalytic activity of iron based heterogeneous Fenton catalyst. Therefore, another motive is to extending the pH range application by new heterogeneous Fenton catalyst. To evaluate the effect of the initial pH on the removal of orange II in the aqueous solution, the FeCu/HMS system, Fe/HMS system and FeCu/MS system with different initial pH values (5.0, 7.0 and 9.0) were set up, while the rest of the operating conditions were unchanged (13.7 mM H_2O_2, 1 g/L catalyst dosage, 30◦C, 50 mg/L orange II). As shown in Fig. 9A and B, the orange II removal efficiencies by FeCu/HMS after 2h of treatment were proximate when executed at different initial pH values. Removal efficiencies of about 93.5 %, 94.3% and 93.8% can be achieved by FeCu/HMS under the initial pH values of 5.0, 7.0 and 9.0, respectively. However, lower orange II removal efficiencies in Fe/HMS system were obtained after 2h of treatment, and their removal efficiencies dropped rapidly from 37.9 % to 29.1 % with an increase of the initial pH value from 5.0 to 9.0. In addition, the removal efficiencies of orange II in FeCu/MS system were 82.7 %, 84.7 % and 84.0 % after 2h when initial pH of dye solution conducted in 5.0, 7.0 and 9.0, respectively. The removal efficiency of orange II by FeCu/MS decreased 2 % and 0.7 % from pH 7.0 to pH 5.0 and pH 9.0, respectively.

The results reveal that the orange II removal efficiency of FeCu/HMS was slightly influenced

by the initial pH compared with Fe/HMS and FeCu/MS. In FeCu/HMS system, the co-operation of copper and iron could improve the reactivity of iron because of the high standard reduction potential difference (0.78 V) between Cu and Fe.[46] Furthermore, the formation of galvanic couple between Cu and Fe could promote the corrosion rate of Fe, which could facilitate the generation of hydroxyl radical (OH•) under oxic conditions.[46,50-51] Moreover, the hollow structure of FeCu/HMS may also play a significant role in pH stability of catalyst. Thus, orange II in an aqueous solution also could be degraded effectively by FeCu/HMS even if the initial pH was 9.0.

3.4. Decomposition of H_2O_2 and generation of hydroxyl radicals for various catalysts

As it known to all, according to Haber-Weiss mechanism,[52,53] hydroxyl radical derives from H_2O_2. Therefore, H_2O_2 decomposition was used to evaluate the performance of different Fenton catalysts.[54,55] The results of H_2O_2 decomposition with different catalysts were shown in Fig. 10A. The lowest activity for H_2O_2 self decomposition (6.0 %) was shown in catalyst free. Moreover, the decomposition rate of H_2O_2 was much higher over FeCu/HMS than that over Fe/HMS. About 38.5 % of H_2O_2 was decomposed in FeCu/HMS, while only 11.9 % of H_2O_2 was decomposed in Fe/HMS. In addition, the decomposition rate of H_2O_2 for FeCu/HMS also was higher than that of FeCu/MS and Cu/HMS, while 32.2 % and 36.4 % of H_2O_2 were decomposed in FeCu/MS and Cu/HMS, respectively. These results agreed with the removing efficiency tendency of orange II under the same conditions.

Hydroxyl radical as a major oxidizing species plays an important role in heterogeneous Fenton process. As previously mentioned, hydroxyl radical derives from H_2O_2. Although the generation of OH• radicals is certainly relevant with H_2O_2 decomposition, the amount of generated •OH radicals is a crucial parameter for evaluating the activity of catalyst. According to the previous literatures,[56,57] the reaction rate constant of benzoic acid reacting with •OH in aqueous media is 4.2

$\times 10^9$ $M^{-1}s^{-1}$ and per mole p-HBA was produced quantitatively by 5.87 ± 0.18 moles •OH. During the analysis, the cumulative amount of •OH radicals were performed by using benzoic acid as a probe and determined through the HPLC. The obtained results were presented in Fig. 10B. The amount of •OH generated by catalysts gradually increase with the reaction time. The amount of •OH generated by FeCu/HMS is up to the highest value about 181.6 μmol L^{-1} after 2 h. It is worthy to note that the capacity of FeCu/HMS to generate •OH is almost 1.6, 2.2, 4.7 and 9.6 times than Cu/HMS (112.8 μmol L^{-1}), FeCu/MS (81.8 μmol L^{-1}), Fe/HMS (38.6 μmol L^{-1}) and catalyst free (18.9 μmol L^{-1}) after 2 h, respectively. However, the decomposition rate of H_2O_2 for FeCu/HMS is just 1.1, 1.2, 3.2 and 6.5 times than Cu/HMS, FeCu/MS, Fe/HMS and catalyst free, respectively, indicating that excellent H_2O_2 utilization efficiency of FeCu/HMS.

3.5 Effect of parameters on catalytic activity of FeCu/HMS for degradation of orange II

3.5.1 Effect of H_2O_2 dosage

The effect of H_2O_2 dosage on the catalytic activity of FeCu/HMS for orange II removal was investigated by conducting experiments at 6.8, 13.7, 27.4, 54.8, 109.6 mM, respectively. As shown in Fig. 11A, B, the degradation of orange II was remarkably accelerated with H_2O_2 concentration increasing from 6.8 to 13.7 mM, especially in the first 15 min reaction time (inset in Fig. 11A). Since H_2O_2 is a source of •OH in the system, more reactive radicals would be produced with the increasing of H_2O_2 concentration.[20] However, when given higher H_2O_2 dosage, the orange II removal was gradually decreased with H_2O_2 dosage from 27.4 to 54.8 mM and obviously dropped down when H_2O_2 dosage is 109.6 mM in the first 15 min reaction time. This is probably due to unavailing consumption of H_2O_2 from the scavenging effect of H_2O_2, which may be described by Eqs. (1) and (2).[22] Based on the above analysis, 13.7 mM H_2O_2 is chosen as the optimal concentration in degradation of orange II.

$H_2O_2 + \bullet OH \rightarrow H_2O + \bullet O_2H$ (1)

$\bullet O_2H + \bullet OH \rightarrow H_2O + O_2$ (2)

3.5.2 Effect of catalyst dosage

The effect of catalyst dosage on the catalytic activity of FeCu/HMS for orange II removal was studied at five different catalyst amounts of 0.25, 0.5, 1.0, 2.0, 3.0 g/L. As depicted in Fig. 11C, D, with catalyst dosage increasing from 0.25 to 1.0 g/L, the removal of orange II efficiency was improved from 79.4 to 94.3 % after 2 h. As we know, the catalyst is the major species to activate H_2O_2 to generate •OH. More dosage of catalyst can provide more active sites and promote higher amount of •OH produced, resulting in an increase of the orange II removal efficiency.[58] However, further increasing catalyst dosage (from 2.0 to 3.0 g/L), the orange II removal efficiency was slightly increased during the first 15 min reaction time (inset in Fig. 11C). Moreover, the final orange II removal efficiency was decreased from 92.9 to 92.5 % after 2h when the catalyst dosage increased from 2.0 to 3.0 g/L. The degradation of removal efficiency may be due to that the excessive catalysts reduced the unit surface adsorption of H_2O_2 and decrease the density of surface adsorbed H_2O_2 on the catalyst surface.[59] Moreover, the •OH radicals may be scavenged by excessive metal species, which was caused by the superfluous catalysts.[60] Based on the above mentioned results, 1.0 g/L of catalyst is chosen as the optimal dosage in degradation of orange II.

3.5.3 Effect of initial dye concentration

The effect of the initial concentration of orange II on the catalytic activity of FeCu/HMS was investigated with five different dye concentrations (50, 100, 200, 300, 400 mg/L). In Fig. 11E, F, it can be observed that the final dye removal efficiency decreased from 94.3 to 72.6 % after 2 h with dye concentration increasing from 50 to 400 mg/L. The results suggest that the removal efficiency of FeCu/HMS was limited by a higher initial concentration of orange II. It may be attributed to

limited reaction area on catalyst, which existed competitive adsorption among dye molecules when conducted in higher concentration of dye.[58] Meanwhile, a higher concentration of intermediates could be generated by a higher initial concentration of orange II, which would decrease the active surface sites available for H_2O_2 and orange II.[46] Despite of this, the total amount of removed orange II increased with the increasing initial dye concentration. Specifically, 47.2, 86.8, 163.2, 236.7, 290.4 mg/L of orange II were removed when initial dye concentration were 50, 100, 200, 300, 400 mg/L, respectively.

3.6. Possible mechanisms

On the basis of all the above experimental results, we proposed a possible mechanism for FeCu/HMS in orange II degradation. In the initial step, Fe^0 is oxidized to Fe^{2+} via a two electron transfer from the nanoparticles surface to H_2O_2 (Eqs. (3)).[7,22] Meanwhile, Cu^0 is oxidized to Cu^+ via a one electron transfer from the nanoparticles surface to H_2O_2 (Eqs. (4)).

$$\equiv Fe^0 + H_2O_2 + 2H^+ \rightarrow \equiv Fe^{2+} + 2H_2O \quad (3)$$

$$2\equiv Cu^0 + H_2O_2 + 2H^+ \rightarrow \equiv 2Cu^+ + 2H_2O \quad (4)$$

Then, Fe^{2+} active H_2O_2 to generate •OH according to the Haber-Weiss mechanism.[52,53] In the mean time, similar with Fe^{2+}, Cu^+ also can active H_2O_2 to generate •OH.[22,61] The reaction equations are presented as follows:

$$\equiv Fe^{2+} + H_2O_2 \rightarrow \equiv Fe^{3+} + \bullet OH + OH^- \quad (5)$$

$$\equiv Fe^{3+} + H_2O_2 \rightarrow \equiv Fe^{2+} + \bullet O_2H + H^+ \quad (6)$$

$$\equiv Cu^+ + H_2O_2 \rightarrow \equiv Cu^{2+} + \bullet OH + OH^- \quad (7)$$

$$\equiv Cu^{2+} + H_2O_2 \rightarrow \equiv Cu^+ + \bullet O_2H + H^+ \quad (8)$$

$$\equiv Fe^{3+} + \equiv Cu^+ \rightarrow \equiv Fe^{2+} + \equiv Cu^{2+}; \quad \Delta E^0 = 0.6\ V \quad (9)$$

Eqs. (9) suggests that the reduction of Fe^{3+} to Fe^{2+} by Cu^+ is thermodynamically favorable due

to the potential difference (0.6 V) between Fe^{3+}/Fe^{2+} (0.77 V) and Cu^{2+}/Cu^{+} (0.17 V).[22,62] Therefore, the interfacial electron transfer is greatly enhanced in FeCu/HMS by redox cycles of Fe^{3+}/Fe^{2+} and Cu^{2+}/Cu^{+} pair.

Moreover, the FeCu/HMS possesses lowest PZC (pH =2.2) according to the observed zeta potential results (Fig. 7), which indicated that most negative charged and most acidic groups occupied at catalyst surface. These functional groups themselves do not promote the •OH radicals generation.[63] However, the more negative surface charges over the catalysts enable to form more H^{+}-concentrated region closed to the catalyst surface.[20,64] On the one hand, more Fe^{2+} and Cu^{2+} facilely to be generated on the surface of catalyst according to Eqs (3) and (4). On the other hand, the protons (H^{+}) over the catalyst surface appear to be in higher concentration compared with bulk aqueous solution.[17] Therefore, the decomposition of adsorbed H_2O_2 into H_2O and O_2 has been greatly suppressed in microscopic localized ambience.[20,65] Consequently, more H_2O_2 would be utilized and react with active sites in a higher •OH radicals generation way via Fenton process.

Furthermore, the hollow structure of FeCu/HMS seems to play a vital role in catalytic activity in heterogeneous Fenton reaction. According to the above catalytic results, FeCu/HMS possesses enhanced catalytic activity than FeCu/MS. The main difference between two catalysts is the support. Particularly, the support of FeCu/HMS is based on three-dimensional hollow mesoporous structure whereas the support of FeCu/MS is based on solid mesoporous structure. The superiority of HMS as support may be attributed to the following reasons. (1) The target molecules (orange II and H_2O_2) were able to facilely diffuse through the silica shell and even reach the interior of hollow space. On this basic, the reactants can contact with Fe-Cu bimetals both from the outside and inside of HMS, which enhance the number of active sites and accelerate the catalytic reaction. (2) The difference of dye concentrations inside and outside facilitates orange II molecules continuing to go inside and

products coming out from the hollow space, which guarantees the continuity of the catalytic reaction. Therefore, the hollow structure of the support makes a significant contribution to excellent catalytic activity of FeCu/HMS.

3.7. The stability and recyclability of catalysts

The stability of FeCu/HMS was evaluated by five consecution experiments at the same conditions, and the results are shown in Fig 12. The used catalysts were collected by magnet after each turn. Then, the collected samples were washed with methanol by ultrasonic and dried for repeated use. Compared to the orange II removal in the first test, the efficiency of catalyst has decreased 13.1 % after the second turn, which may be attributed to the active constituent leaching from the catalyst and catalyst poisoning caused by intermediate products.[66,67] However, it is observed that the catalytic activity of FeCu/HMS remains 78.9 % orange II removal efficiency after five consecutive runs. The results demonstrate that the fabricated FeCu/HMS catalyst shows favorable recyclability performance. On this basic, we proposed that the hollow structure may also provide positive contribution to the stability of FeCu/HMS catalyst, which may be ascribed to the following reasons: the hollow-structured catalyst could be easily separated from the slurry system because of their large weight, weak Brownian motion and good mobility. Moreover, the hollow spheres allow more efficient transport for the reactant molecules to reach the active sites on the framework walls by enabling its reaction with hydroxyl radicals.[68,69]

4. Conclusions

In the present work, an iron-copper bimetal-based hollow mesoporous silica sphere Fenton catalyst was successfully synthesized via a post-impregnation and sodium borohydride reduction strategy. The catalyst possessed a typical hollow mesoporous structure with interior cavity transfixed by mesoporous silica shell and iron-copper nanoparticles highly dispersed in the matrix

of hollow mesoporous silica spheres, which illustrated by XRD, XPS, nitrogen physisorption, SEM, TEM, FT-IR and zeta potential analyses. The enhanced catalytic activity of composite catalyst for orange II removal was observed. It was found that the addition of copper could elevate the catalytic activity, make the catalyst less pH dependent and keep the high activity even at alkaline circumstance. The hollow structure of composite catalyst also played an important role in catalytic activity, due to the positive contribution of "cavity effect". The stability and recoverability of composite catalyst were assessed and exhibited a good performance. The as synthesized composite catalyst was proved to be applied as an attractive alternative in the heterogeneous Fenton catalysis, and the implication of "cavity effect" for catalyst revealed new strategies in the development of novel effective Fenton catalysts.

Acknowledgements

This work was financially supported by the National Natural Science Foundation of China (Grant no. 51478224) and the priority academic program development of Jiangsu higher education institutions.

References

1 E. Brillas, I. Sires, M.A. Oturan, *Chem. Rev.*, 2009, 109, 6570-6631.

2 F.M. Duarte, F.J. Maldonado-Hódar, L.M. Madeira, *Appl. Catal., A*, 2013, 458, 39-47.

3 G. K. Zhang, Y. Y. Gao, Y. L. Zhang, Y. D. Guo, *Environ. Sci. Technol.*, 2010, 44, 6384-6389.

4 Y. L. Zhang, K. Zhang, C. M. Dai, X. F. Zhou, H. P. Si, *Chem. Eng. J.*, 2014, 244, 438-445.

5 X. Zhong, S. Royer, H. Zhang, Q. Q. Huang, L. J. Xiang, S. Valange, J. Barrault, *Sep. Purif. Technol.*, 2011, 80, 163-171.

6 L. G. Devi, K. S. A. Raju, S. G. Kumar, *J. Environ. Monitor.*, 2009, 11, 1397-1404.

7 A. Dhakshinamoorthy, S. Navalon, M. Alvaro, H. Garcia, *Chemsuschem*, 2012, 5, 46-64.

8 E.G. Garrido-Ramírez, B.K.G. Theng, M.L. Mora, *Appl. Clay Sci.,* 2010, 47, 182-192.

9 J. G. Shi, Z. H. Ai, L. Z. Zhang, *Water. Res*., 2014, 59, 145-153.

10 L. G. Devi, K.E. R, K.S. A. Raju, S. G. Kumar, *J. Mol. Catal. A-chem*., 2009, 314, 88-94.

11 L. G. Devi, K.S. A. Raju, S. G. Kumar, K. E. Rajashekhar, *J. Taiwan. Inst. Chem. E.*, 2011, 42, 341-349.

12 Y. Yang, P. Wang, S. J. Shi, Y. Liu, *J. Hazard. Mater*., 2009, 168, 238-245.

13 Z. Eren, N.H. Ince, *J. Hazard. Mater*., 2010, 177, 1019-1024.

14 A.R. Khataee, V. Vatanpour, A.R. Amani Ghadim, Decolorization of C.I. *J. Hazard. Mater*., 2009, 161, 1225-1233.

15 L. Gomathi Devi, S. Girish Kumar, K. Mohan Reddy, C. Munikrishnappa, *J. Hazard. Mater*., 2009, 164, 459-467.

16 J. Y. Cai, H. Ma, J. J. Zhang, Q. Song, Z. T. Du, Y. Z. Huang, J. Xu, *Chem. Eur. J*., 2013, 19, 14215-14223.

17 B. B. Fan, H.Y. Li, W. B. Fan, C. Jin, R. F. Li, *Appl. Catal., A*, 2008, 340, 67-75.

18 M.N. Timofeeva, S.T. Khankhasaeva, E.P. Talsi, V.N. Panchenko, A.V. Golovin, E.T. Dashinamzhilova, S.V. Tsybulya, *Appl. Catal., B*, 2009, 90, 618-627.

19 Z. B. Han, Y. C. Dong, S. M. Dong, *J. Hazard. Mater*., 2011, 189, 241-248.

20 M. Xia, M. C. Long, Y. D. Yang, C. Chen, W. M. Cai, B. X. Zhou, *Appl. Catal., B*, 2011, 110, 118-125.

21 L. Luo, C. Dai, A. Zhang, J. Wang, M. Liu, C. Song and X. Guo, *Catal. Sci. Technol*., 2015.

22 Y. B. Wang, H. Y. Zhao, G. H. Zhao, *Appl. Catal., B*, 2015, 164, 396-406.

23 C.M.A. Parlett, K. Wilson, A.F. Lee, *Chem. Soc. Rev*., 2013, 42, 3876-3893.

24 C. H. Deng, X. Q. Ge, H. M. Hu, L. Yao, C. L. Han, D. F. Zhao, *Crystengcomm*, 2014, 16, 2738-2745.

25 J. C. Chen, Z. T. Xue, S. S. Feng, B. Tu, D. Y. Zhao, *J. Colloid Interface Sci*., 2014, 429, 62-67.

26 X.W. Lou, L.A. Archer, Z. C. Yang, *Adv. Mater*., 2008, 20, 3987-4019.

27 Y. Zhao, L. Jiang, *Adv. Mater*., 2009, 21, 3621-3638.

28 Q. M. Ji, J.P. Hill, K. Ariga, *J. Mater. Chem., A*, 2013, 1, 3600-3606.

29 J. Lee, S.H. Hwang, J. Yun, J. Jang, *ACS Appl. Mater. Interfaces.*, 2014, 6, 15420-15426.

30 S.H. Hwang, D.H. Shin, J. Yun, C. Kim, M. Choi, J. Jang, *Chem. Eur. J.*, 2014, 20, 4439-4446.

31 Z. G. Teng, X. D. Su, Y. Y. Zheng, J. Sun, G. T. Chen, C. C. Tian, J. D. Wang, H. Li, Y. N. Zhao, G. M. Lu, *Chem. Mater.*, 2013, 25, 98-105.

32 M.E. Lindsey, M.A. Tarr, Chemosphere, 2000, 41, 409-417.

33 C. Liu, J. S. Li, J. W. Qi, J. Wang, R. Luo, J. Y. Shen, X. Y. Sun, W. Q. Han, L. J. Wang, *ACS Appl. Mater. Interfaces.*, 2014, 6, 13167-13173.

34 Z. J. Wang, Y. B. Xie, C. J. Liu, *J. Phys. Chem., C*, 2008, 112, 19818-19824.

35 X. F. Li, X. Liu, L. L. Xu, Y. Z. Wen, J. Q. Ma, Z. C. Wu, *Appl. Catal., B*, 2015, 165, 79-86.

36 X. Sun, Y. B. Yan, J. S. Li, W. Q. Han, L. J. Wang, *J. Hazard. Mater.*, 2014, 266, 26-33.

37 X. Zhang, S. Lin, Z. L. Chen, M. Megharaj, R. Naidu, *Water Res.*, 2011, 45, 3481-3488.

38 S. R. Kanel, B. Manning, L. Charlet, H. Choi, *Environ. Sci. Technol.*, 2005, 39, 1291-1298.

39 H. Li, C. Y. Guo, C. L. Xu, *Biosens. Bioelectron.*, 2015, 63, 339-346.

40 K. N.P. Kumar, J. Kumar, K. Keizer, *J. Am. Ceram. Soc.*, 1994, 77, 1396-1400.

41 B.S. Liu, D.F. Xu, J.X. Chu, W. Liu, C.T. Au, *Energ. Fuel.*, 2007, 21, 250-255.

42 Y. H. Ling, M. C. Long, P. D. Hu, Y. Chen, J. W. Huang, *J. Hazard. Mater.*, 2014, 264, 195-202.

43 H. Tamura, K. Mita, A. Tanaka, M. Ito, *J. Colloid Interface Sci.*, 2001, 243, 202-207.

44 C. Moreno-Castilla, M.A. Ferro-Garcia, J.P. Joly, I. Bautista-Toledo, F. Carrasco-Marin, J. Rivera-Utrilla, *Langmuir*, 1995, 11, 4386-4392.

45 F.L.Y. Lam, X. J. Hu, *Catal. Commun.*, 2007, 8, 2125-2129.

46 Y. Yuan, H. Q. Li, B. Lai, P. Yang, M. Gou, Y. X. Zhou, G. Z. Sun, *Ind. Eng. Chem. Res.*, 2014, 53, 2605-2613.

47 L. G. Devi, B. N. Murhty, S. G. Kumar, *Catal. Lett.*, 2009,130, 496-503.

48 L. G. Devi, B. N. Murthy, S. G. Kumar, J. Mol. Catal. A-chem., 2009,308, 174-181.

49 B. Lai, Y. H. Zhang, Z. Y. Chen, P. Yang, Y. X. Zhou, J. L. Wang, Appl. Catal., B, 2014, 144, 816-830

50 L.F. Greenlee, J.D. Torrey, R.L. Amaro, J.M. Shaw, *Environ. Sci. Technol*., 2012, 46, 12913-12920.

51 K. S. Wang, C. L. Lin, M. C. Wei, H. H. Liang, H. C. Li, C. H. Chang, Y. T. Fang, S. H. Chang, *J. Hazard. Mater*., 2010, 182, 886-895.

52 S.S. Lin, M.D. Gurol, *Environ. Sci. Technol*., 1998, 32, 1417-1423.

53 W.P. Kwan, B.M. Voelker, *Environ. Sci. Technol*., 2003, 37, 1150-1158.

53 P. Baldrian, V. Merhautova, J. Gabriel, F. Nerud, P. Stopka, M. Hruby, M.J. Benes, *Appl. Catal., B*, 2006, 66, 258-264.

55 F.C.C. Moura, G.C. Oliveira, M.H. Araujo, J.D. Ardisson, W.A.A. Macedo, R.M. Lago, *Appl. Catal., A*, 2006, 307, 195-204.

56 G.V. Buxton, C.L. Greenstock, W.P. Helman, A.B. Ross, *J. Phys. Chem. Ref. Data.*, 1988, 17, 513-886.

57 Y. J. Wang, H. Y. Zhao, J. X. Gao, G. H. Zhao, Y. G. Zhang, Y. L. Zhang, *J. Phys. Chem. C*., 2012, 116, 7457-7463.

58 C. Cai, H. Zhang, X. Zhong, L. W. Hou, *Water Res*., 2014, 66, 473-485

59 R. X. Huang, Z. Q. Fang, X. M. Yan, W. Cheng, *Chem. Eur. J*., 2012, 197, 242-249

60 X. Y. Zhang, Y. B. Ding, H. Q. Tang, X. Y. Han, L. H. Zhu, N. Wang, *Chem. Eur. J*., 2014, 236, 251-262

61 L. L. Zhang, Y. L. Nie, C. Hu, J. H. Qu, *Appl. Catal., B*, 2012, 125, 418-424.

62 Y. B. Wang, H. Y. Zhao, M. F. Li, J. Q. Fan, G. H. Zhao, *Appl. Catal., B*, 2014, 147, 534-545.

63 J. A. Zazo, A. F. Fraile, A. Rey, A. Bahamonde, J. A. Casas, J. J. Rodriguez, *Catal. Today*., 2009, 143, 341-346.

64 J. Lee, W. Choi, J. Yoon, *Environ. Sci. Technol*., 2005, 39, 6800-6807.

65 L.B. Khalil, B.S. Girgis, T.A.M. Tawfik, *J. Chem. Technol. Biot*., 2001, 76, 1132-1140.

66 J.A. Zazo, J.A. Casas, A.F. Mohedano, J.J. Rodríguez, *Appl. Catal., B*, 2006, 65, 261-268.

67 S. Navalon, M. Alvaro, H. Garcia, *Appl. Catal., B*, 2010, 99, 1-26.

68 S. G. Kumar, K. S. R. K. Rao, *RSC Adv*., 2015, 5, 3306-3351.

69 J. G. Yu, X. X. Yu, *Environ. Sci. Technol*., 2008, 42, 4902-4907.

Figure captions:

Fig. 1. (A) Small-angle and (B) wide-angle XRD patterns of (a) blank HMS, (b) blank MS, (c) FeCu/HMS, (d) FeCu/MS, (e) Fe/HMS and (f) Cu/HMS

Fig. 2. (A) Fe and (B) Cu XPS of (a) blank HMS, (b) blank MS, (c) FeCu/HMS, (d) FeCu/MS, (e) Fe/HMS and (f) Cu/HMS

Fig. 3. SEM and TEM images of (A-C) blank HMS, (D-E) blank MS,

Fig. 4. SEM and TEM images of (A-B) FeCu/HMS, (C-D) FeCu/MS, (E-F) Fe/HMS and (G-H) Cu/HMS

Fig. 5. N_2 adsorption/desorption isotherms (A) and pore size distributions (B) of (a) blank HMS, (b) blank MS, (c) FeCu/HMS, (d) FeCu/MS, (e) Fe/HMS and (f) Cu/HMS

Fig. 6. FTIR spectra of (a) blank HMS, (b) blank MS, (c) FeCu/HMS, (d) FeCu/MS, (e) Fe/HMS and (f) Cu/HMS

Fig. 7. Zeta potential measurements of (a) blank HMS, (b) blank MS, (c) FeCu/HMS, (d) FeCu/MS, (e) Fe/HMS and (f) Cu/HMS

Fig. 8. (A) the remove efficiency of orange II with different catalysts during the reaction in 2h, at pH 7.0 with 13.7 mM H_2O_2, 1g/L catalyst dosage, 50 mg/L orange II , 30 ^oC; (B) the kinetic analysis of orange II degradation with different catalysts, that is the dependence of $\ln(C_0/C)$ versus time.

Fig. 9. The remove efficiency of orange II by FeCu/HMS, Fe/HMS and FeCu/MS with different initial pH values (A) during the reaction in 2h (B) at 2h, with 13.7 mM H_2O_2, 1g/L catalyst dosage, 30 ^oC, 50 mg/L orange II

Fig. 10. Decomposition of H_2O_2 (A) and generation of hydroxyl radicals (B) with different catalysts during the reaction in 2h, at pH 7.0 with 13.7 mM H_2O_2, 1g/L catalyst dosage, 30 ^oC

Fig. 11. Effect of parameters on catalytic activity of FeCu/HMS for degradation of orange II: Effect of H_2O_2 dosage (A) during the reaction in 2h (B) at 2h; Effect of catalyst dosage (C) during the reaction in 2h (D) at 2h; Effect of initial dye concentration (E) during the reaction in 2h (F) at 2h. Except for the investigated parameters, other parameters fixed on pH 7.0 with 13.7 mM H_2O_2, 1g/L catalyst dosage, 50 mg/L orange II , 30 ^oC.

Fig. 12. Degradation of orange II in different batch runs in the FeCu/HMS system

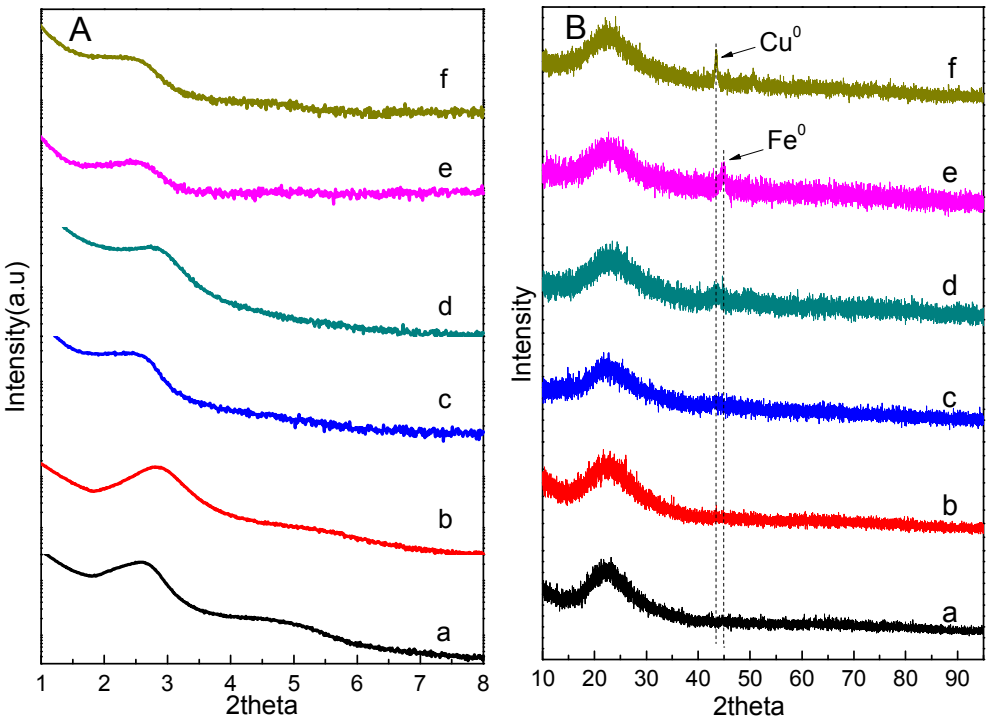

Fig. 1. (A) Small-angle and (B) wide-angle XRD patterns of (a) blank HMS, (b) blank MS, (c) FeCu/HMS, (d) FeCu/MS, (e) Fe/HMS and (f) Cu/HMS

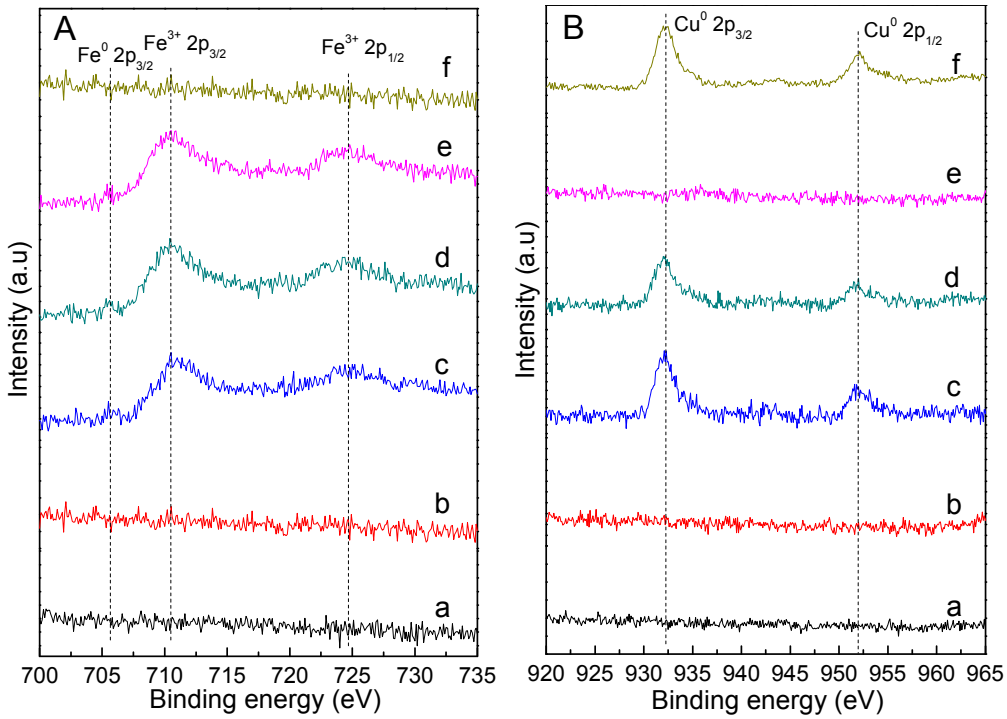

Fig. 2. (A) Fe and (B) Cu XPS of (a) blank HMS, (b) blank MS, (c) FeCu/HMS, (d) FeCu/MS, (e) Fe/HMS and (f) Cu/HMS

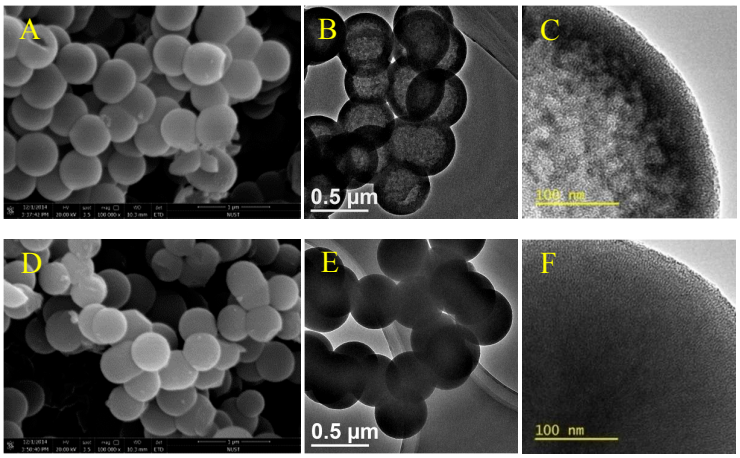

Fig. 3. SEM and TEM images of (A-C) blank HMS, (D-E) blank MS

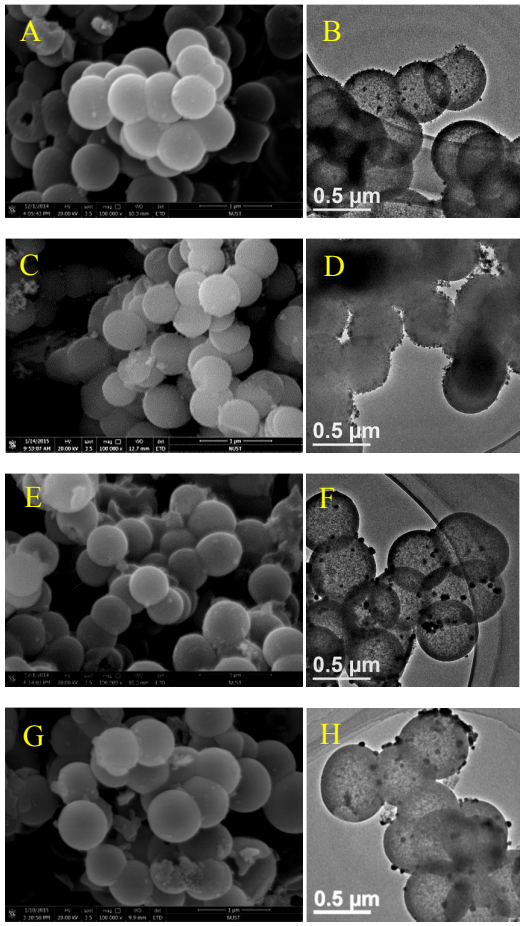

Fig. 4. SEM and TEM images of (A-B) FeCu/HMS, (C-D) FeCu/MS, (E-F) Fe/HMS and (G-H) Cu/HMS

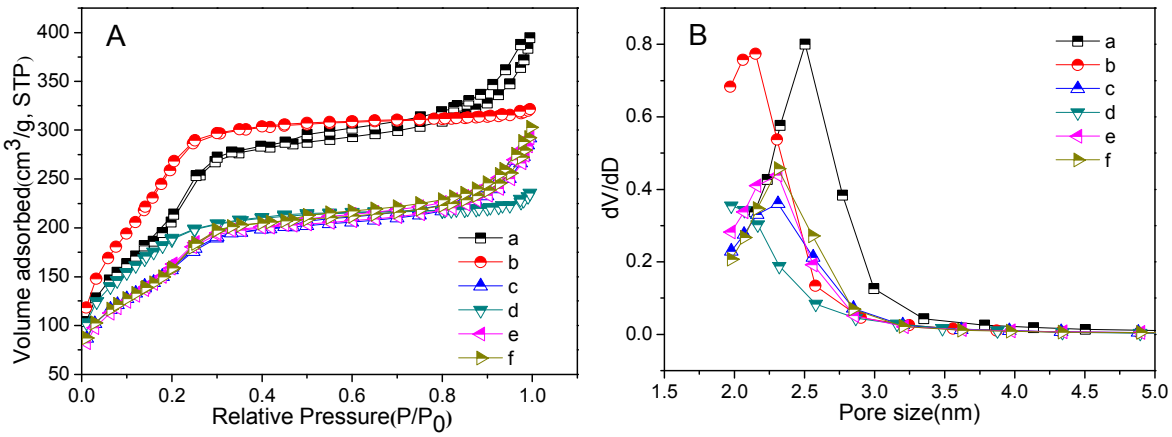

Fig. 5. N_2 adsorption/desorption isotherms (A) and pore size distributions (B) of (a) blank HMS, (b) blank MS, (c) FeCu/HMS, (d) FeCu/MS, (e) Fe/HMS and (f) Cu/HMS

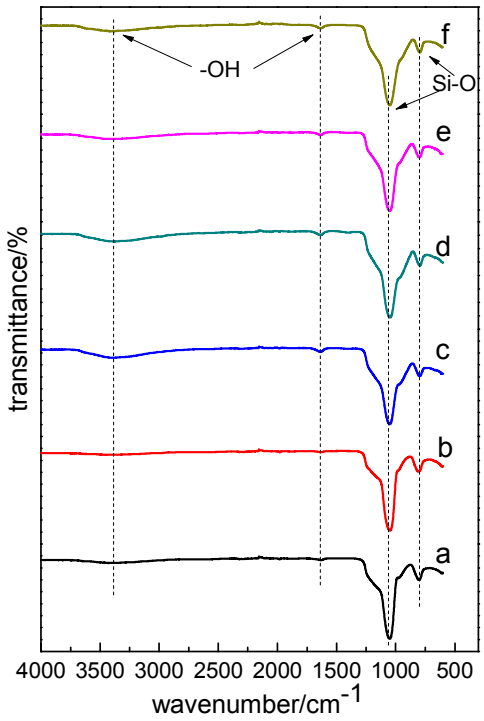

Fig. 6. FTIR spectra of (a) blank HMS, (b) blank MS, (c) FeCu/HMS, (d) FeCu/MS, (e) Fe/HMS and (f) Cu/HMS

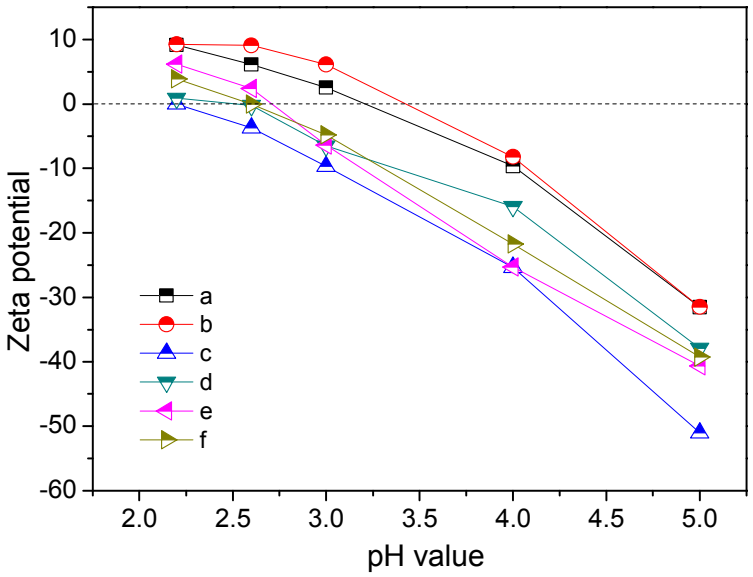

Fig. 7. Zeta potential measurements of (a) blank HMS, (b) blank MS, (c) FeCu/HMS, (d) FeCu/MS, (e) Fe/HMS and (f) Cu/HMS

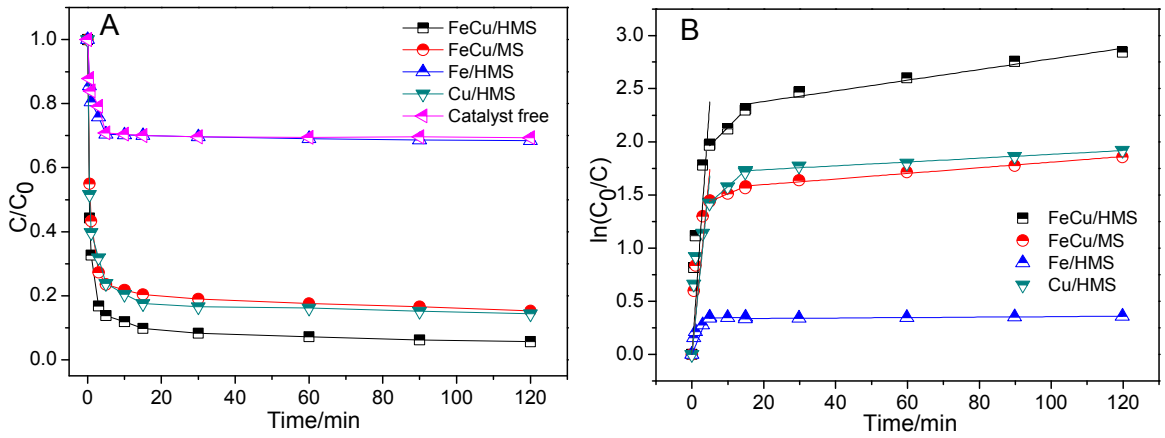

Fig. 8. (A) the remove efficiency of orange II with different catalysts during the reaction in 2h, at pH 7.0 with 13.7 mM H_2O_2, 1g/L catalyst dosage, 50 mg/L orange II , 30 ^oC; (B) the kinetic analysis of orange II degradation with different catalysts, that is the dependence of $ln(C_0/C)$ versus time.

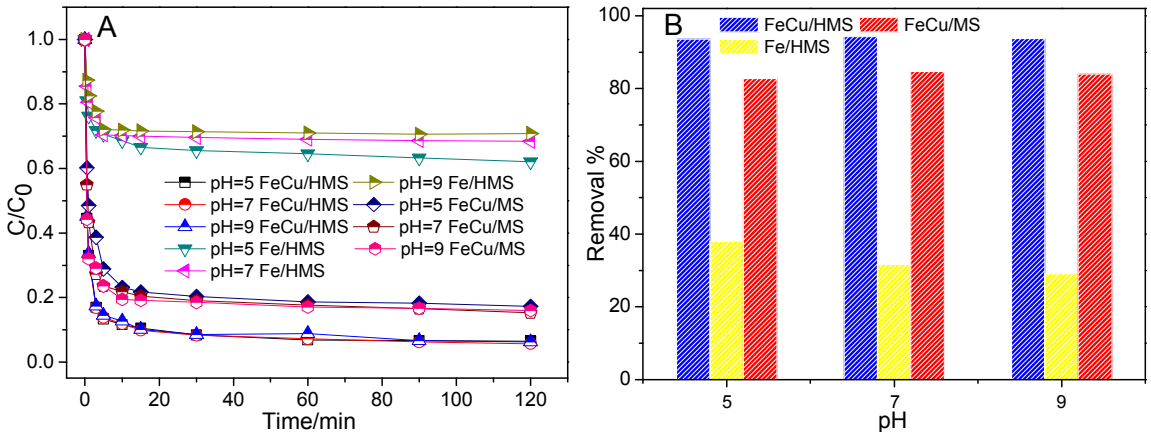

Fig. 9. The remove efficiency of orange II by FeCu/HMS, Fe/HMS and FeCu/MS with different initial pH values (A) during the reaction in 2h (B) at 2h, with 13.7 mM H_2O_2, 1g/L catalyst dosage, 30 ^oC, 50 mg/L orange II

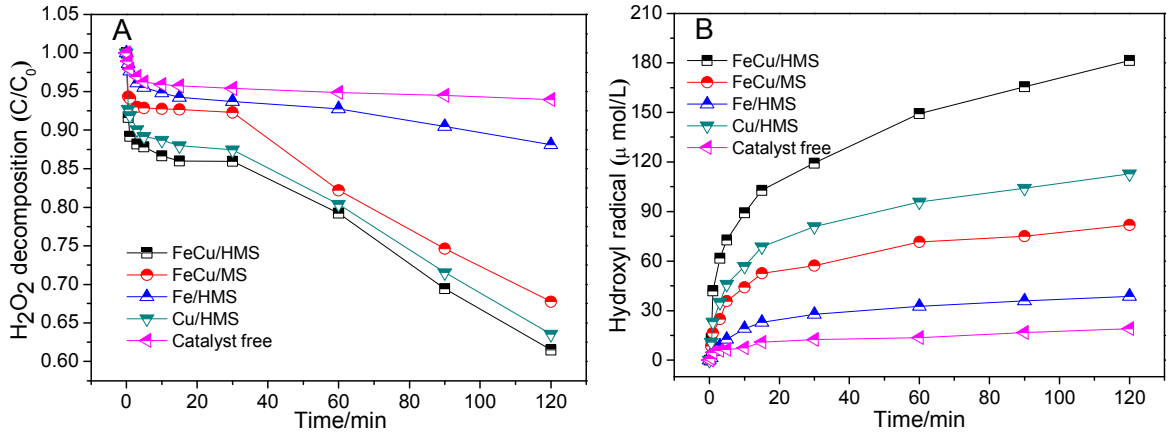

Fig. 10. Decomposition of H_2O_2 (A) and generation of hydroxyl radicals (B) with different catalysts during the reaction in 2h, at pH 7.0 with 13.7 mM H_2O_2, 1g/L catalyst dosage, 30 ^oC

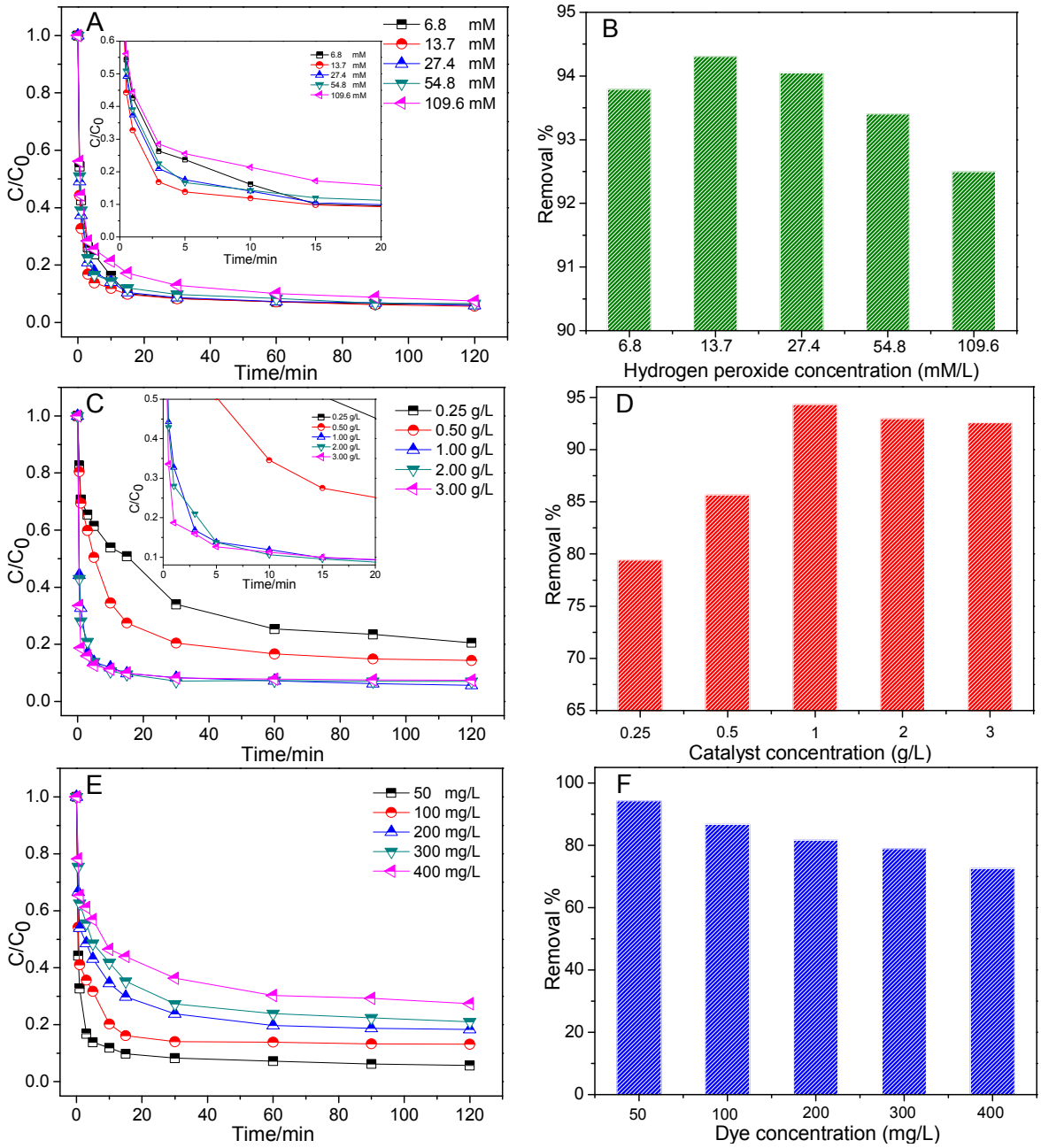

Fig. 11. Effect of parameters on catalytic activity of FeCu/HMS for degradation of orange II: Effect of H_2O_2 dosage (A) during the reaction in 2h (B) at 2h; Effect of catalyst dosage (C) during the reaction in 2h (D) at 2h; Effect of initial dye concentration (E) during the reaction in 2h (F) at 2h. Except for the investigated parameters, other parameters fixed on pH 7.0 with 13.7 mM H_2O_2, 1g/L catalyst dosage, 50 mg/L orange II , 30 ^oC.

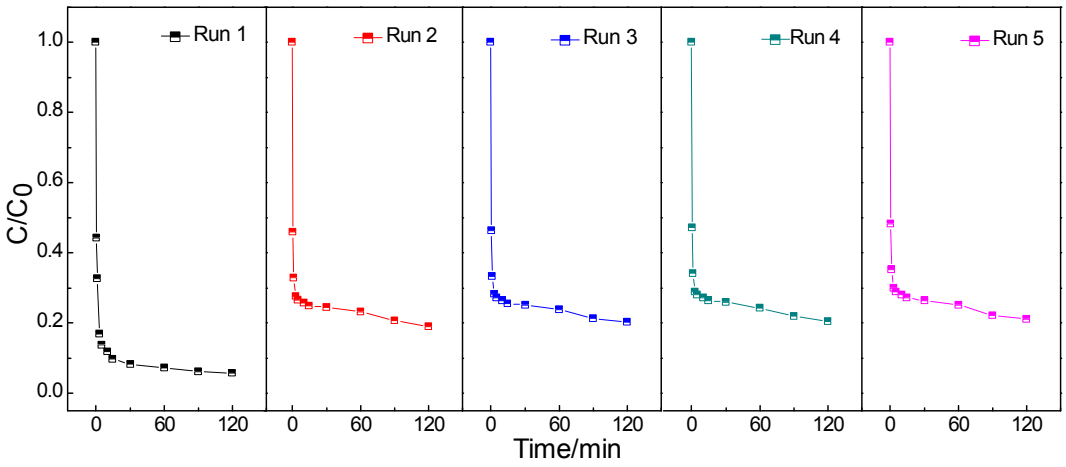

Fig. 12. Degradation of orange II in different batch runs in the FeCu/HMS system

Table 1 Textural properties of synthesized samples.

Sample	S_{BET} $(m^2/g)^{\alpha}$	V_{Total} $(cm^3/g)^{\beta}$	$D_{BJH}(nm)^{\gamma}$
HMS	765	0.56	2.51
MS	1007	0.49	2.13
FeCu/HMS	578	0.41	2.31
FeCu/MS	695	0.35	1.98
Fe/HMS	592	0.41	2.31
Cu/HMS	576	0.41	2.31

α The specific surface areas
β Total pore volume
γ Pore diameter

Table 2 Metal composition in synthesized samples

Sample	Fe content (wt%)	Theoretical value of Fe content(wt%)	Cu content (wt%)	Theoretical value of Cu content(wt%)
HMS	0	0	0	0
MS	0	0	0	0
FeCu/HMS	3.3	3.7	3.4	3.7
FeCu/MS	3.3	3.7	3.4	3.7
Fe/HMS	7.2	7.4	0	0
Cu/HMS	0	0	7.4	7.4

Table 3 Zero potential in synthesized samples

Sample	Zero potential
HMS	3.2
MS	3.4
FeCu/HMS	2.2
FeCu/MS	2.4
Fe/HMS	2.7
Cu/HMS	2.6

Table 4 The reaction kinetics constant of samples

sample	$k_1(min^{-1})$	$k_2(min^{-1})$	$k_3(min^{-1})$
FeCu/HMS	0.4755	0.0342	0.0050
FeCu/MS	0.3478	0.0141	0.0026
Fe/HMS	0.0815	0.0007	0.0002
Cu/HMS	0.3360	0.0306	0.0018

Graphical Abstract